Sensor Location Selection for Continuous Pulp Digesters with Delayed Measurements

Journal:	*AIChE Journal*
Manuscript ID	AIChE-22-24911
Wiley - Manuscript type:	Research Article
Date Submitted by the Author:	22-Mar-2022
Complete List of Authors:	Zhang, Lu Xie, Junyao; University of Alberta, Chemical and Materials Engineering Dubljevic, Stevan; University of Alberta, Chemical and Materials Engineering
Keywords:	Process control, Pulp digester, Kalman filter, Distributed parameter systems

Sensor Location Selection for Continuous Pulp Digesters with Delayed Measurements

Lu Zhang[a], Junyao Xie[a] and Stevan Dubljevic[a,*]

[a]Department of Chemical & Materials Engineering, University of Alberta, Edmonton, AB T6G 2V4, Canada

Abstract

The state estimation and sensor placement for a continuous pulp digester with delayed measurements are investigated. The underlying model of interest is heat transfer in a pulp digester modeled by two coupled hyperbolic partial differential equations and an ordinary differential equation. Output measurements are considered with delay due to the possible low sampling rate. The Cayley-Tustin transformation is utilized to realize model time discretization in a late lumping manner which does not account for any type of spatial approximation or model reduction. The discrete Kalman filter is applied to estimate the system states using the delayed measurements. The selection of sensor location is addressed along with estimator design accounting for the delayed measurements and investigated by minimizing the variance of estimation error. The performance of the state estimator is evaluated, and the sensor placement is analyzed through simulation studies, which provide guidance for sensor location selection in industrial applications.

1 INTRODUCTION

The continuous pulp digester has been predominantly utilized to convert the wood chips into pulp in industrial applications when it comes to the pulping process operation[1]. The typical continuous pulp digester is a complex heterogeneous reactor, consisting of several zones in which the white liquor reacts with wood chips to remove lignin and subsequently free wood fibers[2]. As illustrated in Figure 1, the wood chips and white liquor are added to the impregnation zone where wood chips are soaked by the cooking liquor via penetration and diffusion mechanism. After that, the temperature of the chip mixture is rapidly increased through the external heat exchangers, and the

*Corresponding author: S. Dubljevic. Tel: +1 780 248-1596. Fax: +1 780 492-2881. Email: Stevan.Dubljevic@ualberta.ca.

mixture then enters the cooking zone where the most delignification reactions occur at an elevated temperature. The spent liquor is withdrawn from the digester at extraction screens. At the same time, the cooked pulp moves downwards to the wash zone where the chips are washed and cooled down by the counter-current flow of wash liquor. Finally, the delignification reaction is stopped and the cooked pulp is removed from the bottom of the digester.

Due to the industrial importance the considerable effort has been made in the past few decades to model the delignification process of continuous pulp digesters based on the reaction and diffusion dynamics, and chip-bed compaction. Three widely used dynamic models are known as the Purdue model[3], Gustafson model[4], and Andersson model[5], which have been the bases for the further development of digester models[6, 7, 8, 9]. When it comes to the controller design for the continuous pulp digester, one of the main objectives is to produce pulps that achieve specific quality according to different wood species while respecting distinctive operating conditions. To this end, great efforts have been made to meet various objectives based on the various control methods, such as model predictive control (MPC), adaptive control, dynamic matrix control (DMC), reduced dimension control (RDC), and genetic algorithms (GA) et.al[10, 11, 12, 13, 14].

The state information or the process knowledge is essential for such controllers and/or regulators design. However, the full state information is not often available due to the special features of the continuous digester, physical constraints of sensor installation, and/or the prohibitive expense of implementing spatially-distributed sensors. In addition, some important process variables are sampled infrequently and there are long time delays associated with their measurement. Due to this, the state estimation for the pulp digester attracts a lot of attention in both academia and industry. Along this line, the extended Kalman filter was proposed to construct the true states of a batch pulp digester using online measurements of various liquor characteristics, which shows a good convergence property, even when the state errors and disturbances are undermodeled[11]. The optimal state estimation was realized utilizing the subspace identification techniques and Kalman filter for a continuous digester[15]. The partial least squares methodology was utilized to generate the dynamic model based on input-output data collected from an industrial continuous digester[16]. A multi-rate extended Kalman filter was applied to obtain state estimates that converge to the true plant states in presence of parametric mismatches, unmeasured disturbances and large errors in the initial state estimates[17]. However, even though the aforementioned works have made valuable contributions toward the estimator design for the pulp digester, there are still some aspects which did not receive much attention and consideration. On the one hand, the spatial discretization

of PDE in the estimator design stage dramatically increases the complexity of the calculations in estimator design and might induce numerical instability and/or alter the fundamental control theoretical properties (controllability, observability, stability). On the other hand, the delayed measurement need to be considered because of the possible low sampling rate of the continuous pulp digester.

The accuracy of the estimation depends not only on the type of estimator but also on the location of the sensors, especially for distributed parameter systems. The sensor placement problem has been considered by many researchers in the area of chemical process control, and a number of different performance criteria for sensor placement have been taken into account. One of the earliest approaches is to maximize the observability through a choice of the sensor locations to improve the degree of complete observability for the deterministic state reconstruction problem[18, 19]. For the system with stochastic disturbances, unmeasured states can be estimated with the Kalman filter, and the optimal selection of measurements can be determined by minimizing the average variance of the state estimates[20] or the steady-state error variance[21]. There are also some other criteria to evaluate the performance of sensor locations including detection of load disturbances and location for optimal control[18]. These approaches have mature applications on the lumped parameter systems which are described by ordinary differential equations (ODEs), and have been gradually extended and applied to the DPS in recent years. For example, the modal observability and controllability measures was utilized to determine optimal sensor and actuator locations of parabolic partial differential equations (PDEs)[22]. The optimal area for sensing or actuation in advective PDEs was determined by maximizing the support of the observability or controllability Gramian, respectively[23]. It was demonstrated that the nuclear norm of the solution to the operator Riccati equation is the steady-state minimum error variance of an estimate for distributed parameter systems[24]. The placement of a single sensor and/or a single actuator in advection-diffusion equations with proportional feedback control was addressed[25]. Most of the previous contributions of the sensor selection for distributed parameter systems mainly consider the spectral systems described by parabolic PDEs, which can be addressed by means of model reduction techniques also known in estimation and control theory as the early lumping approach. However, for non-spectral systems (e.g., first order hyperbolic PDEs), where the slow-fast dynamic separation does not hold there are less contributions in the literature. Hence, in this work, the sensor placement for the typical transport-reaction system described by the hyperbolic PDE systems are investigated to motivate and emphasize the issues associated with transport-reaction system setting. First, we consider

the system without state and measurement disturbances, and the observability Gramian can be evaluated in sensor's potential position by solving the Lyapunov equation.

For example, let us consider a simple model of the plug flow reactor with constant transport velocity v and spatial function ψ associated with linearized kinetics of the chemical reaction along the reactor.

$$x_t(z,t) = -v\frac{\partial x(z,t)}{\partial z} + \psi(z)x(z,t) + b(z)u(t) \tag{1a}$$

$$y(t) = \mathcal{C}x(z,t) \tag{1b}$$

$$x(0,t) = 0, x(z,0) = x_0 \tag{1c}$$

where $x(\cdot,t) \in L_2((0,1),\mathbb{R})$ is the system state. The actuation distribution function $b(z)$ is assumed spatially uniform, which accounts for the uniform cooling with the jacket fluid flow. The point measurement is specified with the operator $\mathcal{C}$, which depends on the sensor location l_m, and it can be denoted as $\mathcal{C}(f(z)) = \int_0^l \delta(z-l_m)f(z)d\eta$. One can further define the spatial linear operator $\mathcal{A}(\cdot) = -v\frac{\partial(\cdot)}{\partial z} + \psi(z)(\cdot)$ with a domain $\mathcal{D}(\mathcal{A}) = \{\phi(z) \in L_2(0,1) | \phi(z)$ is abs. cont., $\frac{d\phi}{dz} \in L_2(0,1), \phi(0) = 0\}$, where abs.cont. denotes that ϕ is absolutely continuous.

The observability gramian is well-defined as $L_c\psi = \lim_{\tau\to\infty}\int_0^\tau \mathcal{T}(t)^*\mathcal{C}^*\mathcal{C}\mathcal{T}(t)\psi dt$, where $\mathcal{A}$ generates a C_0 semigroup $\mathcal{T}(t)$. Then, if $\mathcal{T}(t)$ is strongly stable, L_c is the unique solution of the continuous-time observation Lyapunov equation $\mathcal{A}^*L_c\varphi + L_c\mathcal{A}\varphi = -\mathcal{C}^*\mathcal{C}\varphi, \varphi \in \mathcal{D}(\mathcal{A})$, where φ is a spatial function[26]. In order to obtain L_c, the adjoint operator $\mathcal{A}^*$ needs to be found using the inner product formula, $\langle\mathcal{A}\varphi,\phi\rangle = \langle\varphi,\mathcal{A}^*\phi\rangle$, and is $\mathcal{A}^*(\cdot) = -v\frac{\partial(\cdot)}{\partial\zeta} + \psi^*(z)(\cdot)$ with a domain $\mathcal{D}(\mathcal{A}^*) = \{\phi(z) \in L_2(0,1) | \phi(z)$ is abs. cont., $\frac{d\phi}{dz} \in L_2(0,1), \phi(1) = 0\}$. The observability gramian can be obtained further by substituting operators $\mathcal{A}$ and $\mathcal{A}^*$ into the above Lyapunov equation and rearrange as:

$$\frac{\partial L_c}{\partial z} = -\frac{2\psi}{v}L_c - \frac{1}{v}\mathcal{C}^*\mathcal{C}, L_c \in \mathcal{D}(\mathcal{A}^*) \tag{2}$$

Then, the trace norm (nuclear norm) of the observability is utilized to quantify observability for different sensor location, which has been found to be one of the most meaningful measures of observability because it takes the observability of entire system into account[27]. Figure 2 illustrates the relationship between the trace norm of the observability and the single sensor's location along the spatial position. As it is expected, the trace norm of observability gramian increases as the

sensor moves towards the end of the reactor and reaches a maximum at the last point in space. This confirms the application based and practical reasoning that sensor placement at the end of tubular reactor is the best choice. However, when the system is corrupted by disturbances, whether this conclusion still holds, or not, and how the relationship between sensor placement and maximum observability changes are of importance to address especially for hyperbolic PDE systems.

Motivated by the aforementioned issues, this work considers the discrete-time state estimation and sensor placement for stochastic model of continuous pulp digester with delayed boundary/point-wise measurements. The temperature dynamics of a continuous pulp digester is studied, and it is described by coupled PDE-ODE with measurement delay. The Cayley-Tustin time discretization approach is utilized to obtain the discrete-time model with analytical expression that is easier to implement in practical applications. The delayed measurements are expressed by an additional hyperbolic PDE, and treated as the new states of the extended model. The unbounded boundary/ point-wise measurement is considered and can be transformed to a bounded one using Cayley-Tustin approach. The discrete-time Kalman filter is designed with the stochastic discrete-time digester system to realize the state estimation, and the sensor location selection for the temperature measurements is investigated by minimizing the steady-state error variance of the estimated states.

This paper is organized as follows: In Section 2, a dynamic model that describes the temperature system of the cook zone of continuous digester is introduced. The model is discretized in time by utilizing Cayley-Tustin approach. Based on the discrete-time model, the discrete Kalman Filter is designed and the optimal location for the temperature sensors is investigated in Section 3. In Section 4, the performance of the estimator is examined on a number of examples. In Section 5, concluding remarks are made.

2 MODEL FORMULATION FOR PULP DIGESTER

In this section, we introduce the simplified temperature model formulation of a continuous pulp digester. In order to formulate the state-space model, the original model with measurement delay is equivalently transformed to a standard state-space model by introducing the transport PDE. Based on this model, the discrete-time infinite-dimensional model is obtained utilizing the Cayley-Tustin transform framework.

2.1 Model Formulation

Considering that the most of delignification reaction occurs in the cooking zone of a digester[28], we focus on analysis of this zone which can be seen as a vertical tubular reactor of co-current flow in two phases. In addition, the existence of delay in the measurements or sensors is considered, which may be due to slow sampling rate, missing measurement issues, the indirect laboratory analytical test of these measurements, etc. A specified process schematic is shown in Figure 3. The top position of this process is denoted as $z = 0$, and the liquor extraction at the bottom position is denoted as $z = L$. The pre-prenetrated wood chips and free liquor are introduced at the top of the cook zone and the liquor is heated to reaction temperatures achieved by liquor circulation through the cook heater. Therefore, the temperature of heated liquor at the top of the cook zone is selected as the manipulated variable which can be adjusted using the external heater.

The following assumptions are considered. The dynamic variations of chip porosity, the mass variations of solid and liquor, and the variation in external volume flow rate are neglected. The heat released by the exothermic reactions and energy transfer due to diffusion of components between the entrapped liquor phase and free liquor phase can be ignored. Considering the most important components in the chemical reactions taken place in the digester, only lignin in solid phase and effective alkali in liquor phase are taken into account in the reaction rate equations. A further simplification is made by considering only temperature behaviour as neglecting the heat due the reaction makes the temperature variables independent of the concentration variables. For more detail of the model assumptions please refer to the reference[29].

In the ensuing model, the temperature variables are functions of both vertical position z and time t. $T_f(z,t)$ denotes the temperature of free liquor phase, and $T_c(z,t)$ denotes the temperature of chip phase. $T_s(t)$ denotes the free liquor temperature in the steam zone. Based on the aforementioned description, the mathematical model of the temperature behaviour in the cook zone of digester can be modelled by the following set of equations:

$$\frac{\partial T_c}{\partial t} = -\frac{V_c}{A\varepsilon_c}\frac{\partial T_c(z,t)}{\partial z} + U(T_f - T_c)/C_{pe} \tag{3a}$$

$$\frac{\partial T_f}{\partial t} = -\frac{V_f}{A\varepsilon_f}\frac{\partial T_f}{\partial z} - U(T_f - T_c)/C_{pf} \tag{3b}$$

$$\frac{dT_s}{dt} = [-\frac{v_{f,s}}{h_s - h_l} - \frac{k_{lz} - k_{lw}}{C_{pf}\rho_f}]T_s + [\frac{v_{f,s}}{h_s - h_l} + \frac{k_{lz}}{C_{pf}\rho_f}]u + \frac{k_{lw}T_a}{C_{pf}\rho_f} \tag{3c}$$

$$y_m(t) = \begin{bmatrix} T_c(l_{m1}, t-\tau_1) \\ T_f(l_{m2}, t-\tau_2) \end{bmatrix} \tag{3d}$$

The boundary conditions are given by:

$$T_c(0,t) = T_{c0}; T_f(0,t) = T_s(t). \tag{4}$$

where V_c and V_f denote the volume of chip and free liquor respectively, and A is the digester cross sectional area. ε_c is the chip compaction, which increases from the entry through the cook zone, reaching a maximum at the main extraction, $\varepsilon_c(z) = \varepsilon_{10} + \varepsilon_{11} z$, and $\varepsilon_f(z) = 1 - \varepsilon_c(z)$. U denotes the heat-transfer coefficient and relates the rate of energy transfer due to conduction between the wood chips and the free liquor per degree temperature difference per volume of chip[7]. The mixing rules based on weighted averages are utilized to determine heat capacities of the entrapped and free liquor phases, namely, C_{pe} and C_{pf}, which can be further obtained from the heat capacities of the wood C_{ps} and the liquor C_{pl}[30]. $v_{f,s}$ denotes the steam velocity, and h_s and h_l are the height of steam and liquor level, respectively The sensible heat transfer can be written equivalently as $k_{lz}(T_s - u)$, and the heat transfer through the digester shell is $k_{lw}(T_s - T_a)$ where T_a is the ambient temperature. The system input $u(t)$ denotes the steam temperature or the inlet temperature of free liquor at the top of cook zone. The measured output $y_m(t)$ contains the temperature measurement of wood chip and free liquor. Particularly, the time delays (τ_1, τ_2) denote the measurement delays or sensor delays at the bottom of the cook zone. The parameters l_{m1} and l_{m2} represent the sensor locations to measure the temperature of wood chip and free liquor, respectively.

2.2 State-Space Model Formulation

In order to formulate the state-space model, the time delay can be firstly removed at a cost of adding a transport PDE into the plant. Replacing the terms $T_c(l_{m1}, t-\tau_1)$ and $T_f(l_{m2}, t-\tau_2)$ by two transport equations with velocity $\mu_1 := \frac{l_{m1}}{\tau_1}$ and $\mu_2 := \frac{l_{m2}}{\tau_2}$ (e.g.[31, 32]), the original system (Equation (3)) is equivalently expressed as:

$$\frac{\partial T_c}{\partial t} = -\frac{V_c}{A\varepsilon_c}\frac{\partial T_c(z,t)}{\partial z} + U(T_f - T_c)/C_{pe} \tag{5a}$$

$$\frac{\partial T_f}{\partial t} = -\frac{V_f}{A\varepsilon_f}\frac{\partial T_f}{\partial z} - U(T_f - T_c)/C_{pf} \tag{5b}$$

$$\frac{\partial T_w}{\partial t} = -\mu_1 \frac{\partial T_w}{\partial z} \tag{5c}$$

$$\frac{\partial T_v}{\partial t} = -\mu_2 \frac{\partial T_v}{\partial z} \tag{5d}$$

$$\frac{dT_s}{dt} = [-\frac{v_{f,s}}{h_s - h_l} - \frac{k_{lz} - k_{lw}}{C_{pf}\rho_f}]T_s + [\frac{v_{f,s}}{h_s - h_l} + \frac{k_{lz}}{C_{pf}\rho_f}]u + \frac{k_{lw}T_a}{C_{pf}\rho_f} \tag{5e}$$

$$y_m(t) = \begin{bmatrix} T_w(l_{m1}, t) \\ T_v(l_{m2}, t) \end{bmatrix} \tag{5f}$$

The corresponding boundary conditions for this configuration are:

$$\begin{aligned} T_c(0,t) = T_{c0}; T_f(0,t) = T_s(t). \\ T_w(0,t) = T_c(l_{m1}, t); T_v(0,t) = T_f(l_{m2}, t) \end{aligned} \tag{6}$$

Then, the extended state $x(z,t) = [T_c(z,t), T_f(z,t), T_w(z,t), T_v(z,t), T_s(t)]^T = [x_1(z,t), x_2(z,t), x_3(z,t), x_4(z,t), x_5(t)]^T \in \mathcal{X} \bigoplus \mathbb{R}$ is considered, where $\mathcal{X}$ is a real Hilbert spaces $L_2(0,l)^4$ with the inner product $\langle \cdot, \cdot \rangle$, and $\mathbb{R}$ denotes a real space. The input $u(t) \in L^2_{loc}([0,\infty), \mathcal{U})$ and output $y(t) \in L^2_{loc}([0,\infty), \mathcal{Y})$, where $\mathcal{U}$ and $\mathcal{Y}$ are real separable Hilbert spaces. The standard infinite-dimensional continuous-time state-space model can be further formulated as:

$$\dot{x}(z,t) = \mathcal{A}x(z,t) + \mathcal{B}u(t) \tag{7a}$$

$$y(t) = \mathcal{C}x(z,t) \tag{7b}$$

In this form, one can define the system operator $\mathcal{A}(\cdot) = V\frac{\partial(\cdot)}{\partial z} + \psi(z)(\cdot)$ on its domain

$$\mathcal{A}(\cdot) = \begin{bmatrix} -v_c\frac{\partial(\cdot)}{\partial z} + J_{11}(\cdot) & J_{12}(\cdot) & 0 & 0 & 0 \\ J_{21}(\cdot) & -v_f\frac{\partial(\cdot)}{\partial z} + J_{22}(\cdot) & 0 & 0 & 0 \\ 0 & 0 & -\mu_1\frac{\partial(\cdot)}{\partial z} & 0 & 0 \\ 0 & 0 & 0 & -\mu_2\frac{\partial(\cdot)}{\partial z} & 0 \\ 0 & 0 & 0 & 0 & m_1 \end{bmatrix} \tag{8}$$

$$\mathcal{D}(\mathcal{A}) = \left\{ \begin{array}{c} \phi_i(z) \in L_2(0,l)^4, x_5 \in \mathbb{R}: \\ \phi_i(z) \text{ is abs. cont.}, \frac{d\phi_i}{dz} \in L_2(0,l), \text{ with } i = 1,2,3,4, \\ \phi_1(0) = 0, \phi_2(0) = x_5, \phi_3(0) = \phi_1(l_{m1}), \phi_4(0) = \phi_2(l_{m2}) \end{array} \right\} \tag{9}$$

where $v_c = \frac{V_c}{A\varepsilon_c}, v_f = \frac{V_f}{A\varepsilon_f}$, $J_{11} = -U/C_{pe}$, $J_{12} = U/C_{pe}$, $J_{21} = U/C_{pf}$, $J_{22} = -U/C_{pf}$, $m_1 = [-\frac{v_{f,s}}{h_s - h_l} - \frac{k_{lz}-k_{lw}}{C_{pf}\rho_f}]$, $m_2 = [\frac{v_{f,s}}{h_s - h_l} + \frac{k_{lz}}{C_{pf}\rho_f}]$, $m_3 = \frac{k_{lw}T_a}{C_{pf}\rho_f}$. The input operator $\mathcal{B}$ is defined as a

bounded operator $\mathcal{B}$ =[**0**; **0**; **0**; **0**; m_2]. The operator $\mathcal{C}$ is determined as $\mathcal{C}(\cdot) = diag[\mathbf{0}, \mathbf{0}, \int_0^l \delta(z - l_{m1})(\cdot)d\eta, \int_0^l \delta(z - l_{m2})(\cdot)d\eta, \mathbf{0}]$.

In this infinite-dimensional state-space model, there is the uncertainty of operator $\mathcal{C}$ because the sensor locations l_{m1} and l_{m2} need to be determined. Likewise, this also leads to the unknowns of μ_1 and μ_2, which in turn leads to the uncertainty of operator $\mathcal{A}$.

2.3 Model Time-Discretization

Based on the continuous-time infinite-dimensional system, we introduce the Cayley-Tustin discretization framework to transform the continuous system to the discrete-time one. Let us consider the above linear system in Equation (7) and a given a time discretization $h > 0$, and for $j \geq 1$ the Cayley-Tustin discretization is given by

$$\frac{x(jh) - x((j-1)h)}{h} \approx \mathcal{A}\frac{x(jh) + x((j-1)h)}{2} + \mathcal{B}u(jh) \tag{10a}$$

$$y(jh) \approx \mathcal{C}\frac{x(jh) + x((j-1)h)}{2} \tag{10b}$$

with $x(0) = x_0$, where we omit the spatial dependence of x for brevity. Then let $\frac{u_j^{(h)}}{\sqrt{h}}$ be an approximation of $u(jh)$ by the mean value within a given sampling time, $\frac{u_j^{(h)}}{\sqrt{h}} = \frac{1}{h}\int_{(j-1)h}^{jh} u(t)dt$. It has been shown in[33] that $\frac{u_j^{(h)}}{\sqrt{h}}$ converges to $u(jh)$ as $h \to 0$ in several different ways, similar for $Y(jh)$. Further, rewriting Equation (10) gives the discrete time dynamics Equation (11). It is frequently called Tustin discretization in the engineering literature, which is discovered in 1940s by Tustin and referred as Tustin transform in digital and sample-data control literature[34].

$$\frac{x_j^{(h)} - x_{j-1}^{(h)}}{h} \approx \mathcal{A}\frac{x_j^{(h)} + x_{j-1}^{(h)}}{2} + \mathcal{B}\frac{u_j^{(h)}}{\sqrt{h}}, x_0^{(h)} = X_0 \tag{11a}$$

$$\frac{y_j^{(h)}}{\sqrt{h}} \approx \mathcal{C}\frac{x_j^{(h)} + x_{j-1}^{(h)}}{2} \tag{11b}$$

Through some basic computations, the following infinite-dimensional discrete-time state space model is obtained:

$$x_j^{(h)} = \mathcal{A}_d x_{j-1}^{(h)} + \mathcal{B}_d u_j^{(h)} \tag{12a}$$

$$y_j^{(h)} = \mathcal{C}_d x_{j-1}^{(h)} + \mathcal{D}_d u_j^{(h)} \tag{12b}$$

where $\mathcal{A}_d$, $\mathcal{B}_d$, $\mathcal{C}_d$, $\mathcal{D}_d$ are the discrete-time spatial operators and we denote:

$$\begin{pmatrix} \mathcal{A}_d & \mathcal{B}_d \\ \mathcal{C}_d & \mathcal{D}_d \end{pmatrix} = \begin{pmatrix} [\delta - \mathcal{A}]^{-1}[\delta - \mathcal{A}] & \sqrt{2\delta}[\delta - \mathcal{A}]^{-1}\mathcal{B} \\ \sqrt{2\delta}\mathcal{C}[\delta - \mathcal{A}]^{-1} & \mathcal{C}[\delta - \mathcal{A}]^{-1}\mathcal{B} \end{pmatrix} \tag{13}$$

where $\delta = 2/h$ and the resolvent is $\mathcal{R}(\delta, \mathcal{A}) = (\delta I - \mathcal{A})^{-1}$. Clearly, one must satisfy $\delta \in \rho(\mathcal{A})$ so that the resolvent operator is well-defined. In particular, $\mathcal{C}(\delta - \mathcal{A})^{-1}\mathcal{B}$ denotes the transfer function of the continuous model (7). The unbounded operators $\mathcal{A}$ of the continuous-time system are mapped into bounded operators $\mathcal{A}_d$ in the discrete-time counterpart through Cayley transform. In addition, it has been demonstrated that the controllability and stability are invariant under this transformation. The continuous state evolutional operator $\mathcal{A}$ is discretized in time and $\mathcal{A}_d$ can be described by the resolvent operator as follows:

$$\begin{aligned} \mathcal{A}_d(\cdot) &= [\delta I - \mathcal{A}]^{-1}[\delta I + \mathcal{A}](\cdot) \\ &= -I(\cdot) + 2\delta[\delta I - \mathcal{A}]^{-1}(\cdot) \\ &= -I(\cdot) + 2\delta\mathcal{R}(\delta, \mathcal{A})(\cdot) \end{aligned} \tag{14}$$

where I is an identity operator.

2.4 Resolvent operator

From the previous section, one can find the resolvent operator $\mathcal{R}(\delta, \mathcal{A}) = (\delta I - \mathcal{A})^{-1}$ of the system operator $\mathcal{A}$, and then the discrete operators ($\mathcal{A}_d$, $\mathcal{B}_d$, $\mathcal{C}_d$, $\mathcal{D}_d$) can be easily realized. Recalling the continuous-time system model (7), the resolvent operator can be obtained by taking Laplace transform. Under the zero input condition, we can have the following expression:

$$\frac{\partial x_1(z,s)}{\partial z} = \frac{s + J_{11}}{v_c} x_1(z,s) + \frac{J_{12}}{v_c} x_2(z,s) + \frac{1}{v_c} x_1(z,0) \tag{15a}$$

$$\frac{\partial x_2(z,s)}{\partial z} = \frac{s + J_{22}}{v_f} x_2(z,s) + \frac{J_{21}}{v_f} x_1(z,s) + \frac{1}{v_f} x_2(z,0) \tag{15b}$$

$$\frac{\partial x_3(z,s)}{\partial z} = -\frac{s}{\mu_1} x_3(z,s) + \frac{1}{\mu_1} x_3(z,0) \tag{15c}$$

$$\frac{\partial x_4(z,s)}{\partial z} = -\frac{s}{\mu_2} x_4(z,s) + \frac{1}{\mu_2} x_4(z,0) \tag{15d}$$

$$x_b(s) = \frac{1}{s - m_1} x_b(0) \tag{15e}$$

By solving the above ODE, a frequency-domain solution of the distributed digester system is finally obtained as follows:

$$\begin{bmatrix} x_1(z,s) \\ x_2(z,s) \end{bmatrix} = e^{Mz} \begin{bmatrix} x_1(0,s) \\ x_2(0,s) \end{bmatrix} - \int_0^z e^{M(z-\eta)} V_0^{-1} \begin{bmatrix} x_1(\eta,0) \\ x_2(\eta,0) \end{bmatrix} d\eta \tag{16a}$$

$$x_3(z,s) = e^{-\frac{s}{\mu_1}z} x_3(0,s) + \int_0^z e^{-\frac{s}{\mu_1}(z-\eta)} x_3(\eta,0) d\eta \tag{16b}$$

$$x_4(z,s) = e^{-\frac{s}{\mu_2}z} x_4(0,s) + \int_0^z e^{-\frac{s}{\mu_2}(z-\eta)} x_4(\eta,0) d\eta \tag{16c}$$

where

$$V_0 = \begin{bmatrix} -v_c & 0 \\ 0 & -v_f \end{bmatrix}, B_0 = \begin{bmatrix} s - J_{11} & -J_{12} \\ -J_{21} & s - J_{22} \end{bmatrix}, M = V_0^{-1} B_0 \tag{17}$$

For simplicity, one can introduce the following notations in order to determine the resolvent operator:

$$e^{Mz} = \begin{bmatrix} M_{11}(z,s) & M_{12}(z,s) \\ M_{21}(z,s) & M_{22}(z,s) \end{bmatrix} \tag{18}$$

After further manipulations, the closed-form analytical solutions of the state evolution matrix can be arranged as follows:

$$\begin{cases} M_{11}(z,s) = e^{\frac{Gz}{2v_c v_f}} \left[\frac{K}{F} \sinh(\frac{Fz}{2v_c v_f}) + \cosh(\frac{Fz}{2v_c v_f}) \right] \\ M_{12}(z,s) = \frac{2J_{12}v_f}{F} e^{\frac{Gz}{2v_c v_f}} \sinh(\frac{Fz}{2v_c v_f}) \\ M_{21}(z,s) = \frac{2J_{21}v_c}{F} e^{\frac{Gz}{2v_c v_f}} \sinh(\frac{Fz}{2v_c v_f}) \\ M_{22}(z,s) = e^{\frac{Gz}{2v_c v_f}} \left[-\frac{K}{F} \sinh(\frac{Fz}{2v_c v_f}) + \cosh(\frac{Fz}{2v_c v_f}) \right] \end{cases} \tag{19}$$

where F, G, K are denoted as:

$$F = \sqrt{(J_{11}-s)^2 v_f^2 + 2v_c v_f (2J_{12}J_{21} + (J_{11}-s)(s-J_{22})) + (J_{22}-s)^2 v_c^2}$$

$$G = J_{11}v_f + J_{22}v_c - s(v_c + v_f)$$

$$K = J_{11}v_f - J_{22}v_c + s(v_f - v_c)$$

Therefore, with the boundary conditions given by $x_3(0,s) = x_1(l_{m1},s)$ and $x_4(0,s) = x_4(l_{m2},s)$, $x_3(z,s)$ and $x_4(z,s)$ can be obtained. The resolvent operator can be expressed as follows:

$$x(z,s) = \mathcal{R}(s,\mathcal{A}) x(\eta,0) \tag{20}$$

where

$$\mathcal{R}(s,\mathcal{A}) = \begin{bmatrix} \mathcal{R}_{11} & \mathcal{R}_{12} & 0 & 0 & \mathcal{R}_{15} \\ \mathcal{R}_{21} & \mathcal{R}_{22} & 0 & 0 & \mathcal{R}_{25} \\ \mathcal{R}_{31} & \mathcal{R}_{32} & \mathcal{R}_{33} & 0 & \mathcal{R}_{35} \\ \mathcal{R}_{41} & \mathcal{R}_{42} & 0 & \mathcal{R}_{44} & \mathcal{R}_{45} \\ 0 & 0 & 0 & 0 & \mathcal{R}_{55} \end{bmatrix} \tag{21}$$

where

$$\begin{cases} \mathcal{R}_{i1}(\cdot) = \int_0^z \frac{1}{v_c} M_{i1}(z-\eta,s)(\cdot)d\eta, i=1,2 \\ \mathcal{R}_{i2}(\cdot) = \int_0^z \frac{1}{v_f} M_{i2}(z-\eta,s)(\cdot)d\eta, i=1,2 \\ \mathcal{R}_{i5}(\cdot) = \frac{M_{i2}(z,s)}{s-m_1}(\cdot), i=1,2 \\ \mathcal{R}_{31}(\cdot) = e^{-\frac{s}{\mu_1}z} \int_0^{l_{m1}} \frac{1}{v_c} M_{11}(l_{m1}-\eta,s)(\cdot)d\eta \\ \mathcal{R}_{32}(\cdot) = e^{-\frac{s}{\mu_1}z} \int_0^{l_{m1}} \frac{1}{v_f} M_{12}(l_{m1}-\eta,s)(\cdot)d\eta \\ \mathcal{R}_{33}(\cdot) = \int_0^z e^{-\frac{s}{\mu_1}(z-\eta)} \frac{1}{\mu_1}(\cdot)d\eta \\ \mathcal{R}_{35}(\cdot) = e^{-\frac{s}{\mu_1}z} \frac{M_{12}(l_{m1},s)}{s-m_1}(\cdot) \\ \mathcal{R}_{41}(\cdot) = e^{-\frac{s}{\mu_2}z} \int_0^{l_{m2}} \frac{1}{v_c} M_{21}(l_{m2}-\eta,s)(\cdot)d\eta \\ \mathcal{R}_{42}(\cdot) = e^{-\frac{s}{\mu_2}z} \int_0^{l_{m2}} \frac{1}{v_f} M_{22}(l_{m2}-\eta,s)(\cdot)d\eta \\ \mathcal{R}_{44}(\cdot) = \int_0^z e^{-\frac{s}{\mu_2}(z-\eta)} \frac{1}{\mu_2}(\cdot)d\eta \\ \mathcal{R}_{45}(\cdot) = e^{-\frac{s}{\mu_2}z} \frac{M_{22}(l_{m2},s)}{s-m_1}(\cdot) \\ \mathcal{R}_{55}(\cdot) = \frac{1}{s-m_1}(\cdot) \end{cases} \tag{22}$$

Now, the discrete-time operators in Equation (13) can be solved by straightforwardly substituting the above resolvent operators. Afterwards, the discrete-time linear model is obtained:

$$x(z,k) = \mathcal{A}_d x(z,k-1) + \mathcal{B}_d u(k) \tag{23a}$$

$$y(k) = \mathcal{C}_d x(z,k-1) + \mathcal{D}_d u(k) \tag{23b}$$

with the boundary conditions Equation (6). It is worth noting that the uncertainty of the sensor location l_{m1} and l_{m2} will lead to the uncertainty of the resolvent operator and then further effects on the operators $\mathcal{A}_d$, $\mathcal{B}_d$, $\mathcal{C}_d$ and $\mathcal{D}_d$.

3 State Estimation and Sensor Placement for the Stochastic system

3.1 Discrete Stochastic Model Formulation

In order to account for the process and measurement noise of the digester, the Kalman filter is developed as an one-step ahead predictor. In this case, one can introduce the bounded operators G_w accounting for spatial influence of state noise ω_k at each time instance. By assuming that there is no prior knowledge of the noise source, the discrete-time digester system with addictive disturbances/noises is considered in the following form:

$$x_k = \mathcal{A}_d x_{k-1} + \mathcal{B}_d u_k + G_w \omega_k \tag{24a}$$

$$y_k = \mathcal{C}_d x_{k-1} + \mathcal{D}_d u_k + v_k \tag{24b}$$

where ω_k denotes process noise, which is the zero mean multivariate normal distribution with covariance Q_k given as $\omega_k \sim \mathcal{N}(0, Q_k)$, $E[\omega_k \omega_j^T] = Q_k \delta_{k,j}$, and $\delta_{k,j}$ is the Dirac delta function, i.e., $\delta_{k,j} = 1$ if $k = j$ and $\delta_{k,j} = 0$ otherwise, while v_k represents measurement noise at time step k of having zero mean Gaussian white noise with covariance R_k denoted as $v_k \sim \mathcal{N}(0, R_k)$, $E[v_k v_j^T] = R_k \delta_{k,j}$, and $E[v_k \omega_j^T] = 0$. Furthermore, we consider independent process noise and measurement noise. In order to guarantee the consistency in the time instants of the discrete digester system and the standard discrete Kalman filter structure in finite-dimensional setting, one can express y_k by the state x_k instead of x_{k-1} in Equation (23) and Equation (24), which yields the following:

$$x_k = \mathcal{A}_d x_{k-1} + \mathcal{B}_d u_k + G_w \omega_k \tag{25a}$$

$$y_k = \bar{\mathcal{C}}_d x_k + \bar{\mathcal{D}}_d u_k + v_k \tag{25b}$$

where the associated discrete-time spatial operators are denoted as follows[35]:

$$\begin{pmatrix} \mathcal{A}_d & \mathcal{B}_d & G_w \\ \bar{\mathcal{C}}_d & \bar{\mathcal{D}}_d & - \end{pmatrix} = \begin{pmatrix} -I + 2\delta \mathcal{R}(z,\delta) & \sqrt{2\delta}\mathcal{R}(z,\delta)\mathcal{B} & \sqrt{2\delta}\mathcal{R}(z,\delta)G \\ -\sqrt{2\delta}\mathcal{C}\mathcal{R}(z,-\delta) & \mathcal{G}(-\delta) & - \end{pmatrix} \tag{26}$$

3.2 Discrete Kalman Filter Design

In this section, a classical discrete-time Kalman filter is designed for the well-defined stochastic discrete-time digester system (24). Kalman filter is often realized in two steps, including a prediction step and an updating step, also referred as a priori estimation step and a posteriori estimation step[36]. Firstly, the following notations are introduced.

$$\begin{aligned} \hat{x}_k^- &= E[x_k \mid y_1, y_2, ..., y_{k-1}] = \text{a priori estimate} \\ \hat{x}_k^+ &= E[x_k \mid y_1, y_2, ..., y_k] = \text{a posteriori estimate} \end{aligned} \tag{27}$$

In addition, we use the term P_k to denote the covariance of the estimation error. P_k^- denotes the covariance of the estimation error of $\hat{x}_k^-$, $P_k^- = E[(x_k - \hat{x}_k^-)(x_k - \hat{x}_k^-)^*]$, and P_k^+ denotes the covariance of the estimation error of $\hat{x}_k^+$, $P_k^+ = E[(x_k - \hat{x}_k^+)(x_k - \hat{x}_k^+)^*]$.

We begin the estimation process with the guess of initial conditions which are described as below:

$$\begin{cases} \hat{x}_0^+ = E(x_0) = \hat{x}_0 \\ P_0^+ = E[(x_0 - \hat{x}_0^+)(x_0 - \hat{x}_0^+)^*] = Q_0 \end{cases} \tag{28}$$

Then, one has the following prior estimation or prediction step, with measurement up to time $k-1$:

$$\begin{cases} P_k^- = \mathcal{A}_d P_{k-1}^+ \mathcal{A}_d^* + G_w Q_{k-1} G_w^* = \mathcal{A}_d (\mathcal{A}_d P_{k-1}^+)^* + G_w Q_{k-1} G_w^* \\ \hat{x}_k^- = \mathcal{A}_d \hat{x}_{k-1}^+ + \mathcal{B}_d u_k \end{cases} \tag{29}$$

The posterior estimation or update step is given as follows, by using additional output measurement y_k at time instance k:

$$\begin{cases} K_k = P_k^- \bar{\mathcal{C}}_d^* (\bar{\mathcal{C}}_d P_k^- \bar{\mathcal{C}}_d^* + R_k)^{-1} = (\bar{\mathcal{C}}_d P_k^-)^* [\bar{\mathcal{C}}_d (\bar{\mathcal{C}}_d P_k^-)^* + R_k]^{-1} \\ P_k^+ = (I - K_k \bar{\mathcal{C}}_d) P_k^- (I - K_k \bar{\mathcal{C}}_d)^* + K_k R_k K_k^* \\ \quad = I P_k^- I^* - K_k \bar{\mathcal{C}}_d P_k^- I^* - I P_k^- \bar{\mathcal{C}}_d^* K_k^* + K_k \bar{\mathcal{C}}_d P_k^- \bar{\mathcal{C}}_d^* K_k^* + K_k R_k K_k^* \\ \quad = I P_k^- I^* - K_k \bar{\mathcal{C}}_d P_k^- I^* - I (\bar{\mathcal{C}}_d P_k^-)^* K_k^* + K_k \bar{\mathcal{C}}_d (\bar{\mathcal{C}}_d P_k^-)^* K_k^* + K_k R_k K_k^* \\ \hat{x}_k^+ = \hat{x}_k^- + K_k (y_k - \bar{\mathcal{C}}_d \hat{x}_k^- - \bar{\mathcal{D}}_d u_k) \end{cases} \tag{30}$$

The basic configuration extends a standard discrete-time finite-dimensional Kalman filter design algorithm[36]. Compared to the general matrix forms of state space representation in finite-dimensional systems, the discrete spatial operators $(\mathcal{A}_d, \mathcal{B}_d, \bar{\mathcal{C}}_d, \bar{\mathcal{D}}_d, G_w)$ need to be treated carefully as they are induced by Cayley-Tustin time discretization. In addition, the covariances P_k^- and P_k^+

are two-dimensional and self-adjoint with spatial characteristics.

3.3 Optimal Sensor Location

The basic idea of optimal sensor selection is to select the locations of sensor among a given finite location set, which provides as much information of the dynamic system as possible. To realize this goal, the optimal sensor selection can be formulated as an optimization problem, aiming to minimize a given objective function related to the dynamic characteristics of the system. In this paper, the objective is to minimize the steady-state error variance of the estimated states, which is in the nuclear norm[24]. The value of steady-state error variance is dependent on the measurement operator $\mathcal{C}$, and hence on the number of sensors, as well as on the sensor noise covariance R_k. Thus, minimizing the steady-state error variance is a reasonable design goal when it comes to the sensor location selection. The sensor locations are defined as the discrete optimization variables and the constraints are typically the given sensor number.

$$\min_{\vartheta \in \Omega^n} \ \|P_{ss}(\vartheta)\|_1 \tag{31a}$$

$$\text{s.t.} \ \ g(\vartheta) = n, \tag{31b}$$

$$\vartheta^{lb} \leq \vartheta \leq \vartheta^{ub}, \tag{31c}$$

$$\vartheta \in \mathbb{Z}^+. \tag{31d}$$

where $\vartheta = \{\theta_1, \theta_2, ..., \theta_n\}$ represents the sensor locations defined by a set of integers, $\|P_{ss}(\vartheta)\|_1$ is the nuclear norm of steady-state error variance, $g(\vartheta)$ denotes the total number of sensor locations, n is the given sensor number, ϑ^{lb} and ϑ^{ub} are the lower and upper bounds of ϑ, respectively, and $\mathbb{Z}^+$ denotes the set of positive integers. The minimum solution of Equation (31) is then the optimal sensor configuration as follows:

$$\vartheta^* = arg \min_{\vartheta \in \Omega^n} \ \|P_{ss}(\vartheta)\|_1 \tag{32a}$$

$$\text{s.t.} \ \ g(\vartheta) = n, \tag{32b}$$

$$\vartheta^{lb} \leq \vartheta \leq \vartheta^{ub}, \tag{32c}$$

$$\vartheta \in \mathbb{Z}^+. \tag{32d}$$

Problem (32) can be solved by the following procedure.

1) determine the feasible sensor location set Ω^n

2) For every sensor configuration $\vartheta \in \Omega^n$, solve the problem (32).

3) The optimal sensor location of the considered system is obtained as ϑ^*.

4 SIMULATION RESULTS

In this section, we provide numerical examples associated with the discrete-time Kalman filter design and sensor selection. First, we revisit the motivation example discussed in Section 1 to demonstrate the performance of the proposed filter and compare the results of sensor location by using different criteria, including maximum observability and minimum variance estimation. Then, the developed infinite-dimensional discrete-time Kalman filter for the digester system is simulated and the corresponding results are discussed in detail. Two cases are further considered, including the spatially distributed process noise and the spatially centered process noise. The numerical simulation is further investigated to determine the optimal sensor placement, which might provide a guidance for sensor location selection and efficient monitoring of digester systems in practice.

4.1 Motivation Example Revisited

In this section, the proposed Kalman filter design and sensor selection are applied to the scalar hyperbolic system presented in Section 1. The discrete-time linear hyperbolic PDE system corresponding to Equation (1) is obtained by applying Cayley-Tustin transformation and is given in the following form:

$$x(z,k) = \mathcal{A}_d x(z,k-1) + \mathcal{B}_d u(k) + \omega(k), x(z,0) = x_0 \tag{33a}$$

$$y(k) = \mathcal{C}_d x(z,k) + \mathcal{D}_d u(k) + v(k) \tag{33b}$$

where

$$\begin{cases} \mathcal{A}_d(\cdot) = [\delta I - \mathcal{A}]^{-1}[\delta I + \mathcal{A}](\cdot) \\ \qquad = -I(\cdot) + 2\delta \left[\int_0^z \frac{1}{v}(\cdot) e^{-\frac{1}{v}(\psi-\delta)\eta} d\eta\right] e^{\frac{1}{v}(\psi-\delta)z} \\ \mathcal{B}_d = \sqrt{2\delta}[\delta I - \mathcal{A}]^{-1}\mathcal{B}(z) \\ \quad = \sqrt{2\delta}\left[\int_0^z \frac{1}{v}\mathcal{B}(\eta) e^{-\frac{1}{v}(\psi-\delta)\eta} d\eta\right] e^{\frac{1}{v}(\psi-\delta)z} \\ \mathcal{C}_d(\cdot) = -\sqrt{2\delta}\mathcal{C}[-\delta I - \mathcal{A}]^{-1}(\cdot) \\ \qquad = -\sqrt{2\delta}\left[\int_0^{l_m} \frac{1}{v}(\cdot) e^{-\frac{1}{v}(\psi+\delta)\eta} d\eta\right] e^{\frac{1}{v}(\psi+\delta)l_m} \\ \mathcal{D}_d = \mathcal{C}[-\delta I - \mathcal{A}]^{-1}\mathcal{B} + \mathcal{D} \\ \qquad = \left[\int_0^{l_m} \frac{1}{v}\mathcal{B}(\eta) e^{-\frac{1}{v}(\psi+\delta)\eta} d\eta\right] e^{\frac{1}{v}(\psi+\delta)l_m} \end{cases} \tag{34}$$

The simulation result of the Kalman filter design given Equations (28)-(30) for the discrete scalar hyperbolic PDE system is shown in Figure 4. In this case, the spatial parameter in the operator A is chosen to be $\psi = 0.5$, while the input operator $B(0 < z < 1) = 1$ represents spatially uniform realized heat transfer across the reactor shell. The time varying input is considered as $u(k) = 3sin(2\pi k)$, the potential position of the sensor location is considered as $[0.05, 0.1, 0.2, 0.3, 0.4, 0.5, 0.6, 0.7, 0.8, 0.9, 1]$. The initial conditions are taken as $x_0 = 5sin(2\pi z)$ and $\hat{x}_0 = 3sin(4\pi z)$. The process noise and measurement noise are considered as $\omega_k \sim \mathcal{N}(0, Q_k)$ with $Q_k = 0.05$, and $v_k \sim \mathcal{N}(0, R_k)$ with $R_k = 0.1$.

The evolution profiles of the trace of two-dimensional estimate covariance along the time instance at each potential position of the sensor are shown in Figure 5. The trace norm profiles are able to converge to the steady state after 1 second. The steady state of the trace norm of estimation error covariance subject to the location of the sensor is shown in Figure 6, which also shows the profile of the trace of observability. It is clear that the trace norm of observability increases roughly linearly with the movement of the sensor position, and reaches the maximum at the end. However, the trace norm of estimation covariance shows roughly a quadratic relationship with the sensor location and reaches the minimum point at 0.7. The results indicate that for the scalar hyperbolic PDE, maximizing observability does not generally guarantee the minimum variance estimation. In the other words, it also implies that the maximum observability is not the best criteria for the sensor location from minimizing estimation error view point.

4.2 Performance of State Estimation and Sensor Selection for Pulp Digester

The values of all system parameters and for simulations are listed in Table 1. For the initial conditions of the dynamic system, we consider $x_1(z, 0) = 0.18\sin(0.4\pi z), x_2(z, 0) = 0.87\sin(0.4\pi z)$.

As for the Cayley-Tustin time discretization, we choose $h = 2s$ at the time discretization interval. The spatial discretization interval is taken as $\Delta z = 0.05$. The time delays (τ_1, τ_2) are considered as $(0.05, 0.05)$. Firstly, the open-loop temperature model of cook zone is simulated in Figure 7 with the activated control action $u(t) = 4\sin(0.05t)$. It is apparent that the state evolution profile behaves follow the periodic wave trend induced by the given input.

4.2.1 Performance of Discrete Kalman Filter

In this case, the developed discrete-time Kalman filter configuration is applied to the stochastic linear infinite-dimensional discrete-time digester system (25), and the performance is analyzed. In addition, the sensor location is first considered at the bottom of cook zone, that means $l_{m1} = l_{m2} = l$. Based on that, two different disturbances are considered: spatially distributed and centered disturbance. In both cases, the plant and measurement noises, we take $\omega_k \sim \mathcal{N}(0, Q_k)$, $E[\omega_k \omega_j^T] = Q_k \delta_{k,j}$, $v_k \sim \mathcal{N}(0, R_k)$, $E[v_k v_j^T] = R_k \delta_{k,j}$, $E[v_k \omega_j^T] = 0$ with $Q_k = 0.005$ and $R_k = diag(1, 2)$. The initial conditions are taken as $x_1(z, 0) = 0.18sin(0.4\pi z)$ and $x_2(z, 0) = 0.9sin(0.4\pi z)$, and the control action are given as $u(t) = 4sin(0.05t)$, and the estimated initial conditions are $\hat{x}_1(z, 0) = 0.16sin(0.4\pi z)$ and $\hat{x}_2(z, 0) = 0.8sin(0.4\pi z)$.

Case 1: Spatially distributed process noise

In this case, the spatially distributed noise is considered first for the description of the noise on the state distribution in the spatial domain, which is defined as $g(z) = 1 + 30sech(100(z - 0.2))$, and the operator is defined as $G(z) = [\mathbf{1}, \mathbf{1}, \mathbf{1}, \mathbf{1}, \mathbf{1}]^T$.

Profiles of the state with noise and the estimated state are presented in Figure 8 and Figure 9. Compared with Figure 7 , it can be seen that there are some noisy oscillations in the two states induced by the process noise and measurement noise, and the developed Kalman filter is capable of reconstructing the entire spatiotemporal state profile and reducing noises present in the process and measurement simultaneously. Moreover, in Figure 10 the profiles of the noisy outputs, the estimated outputs, and the real outputs are presented. The filtered output of interest matches perfectly with the one in the noise-free system, with largely eliminating the noises involved in the stochastic digester system. The measurement error and the estimation error are utilized to evaluate the estimation accuracy of the designed Kalman filter, as shown in Figure 11.

Case 2: Spatially centered process noise

In this case, the spatially centered process noise is considered and we assume the noise only appears in the temperature of wood chips. The centered disturbance illustrated as function $g(z) =$

$20sech(100(z-0.2))$, and the operator is defined as $G(z) = [g(z), \mathbf{0}, g(z), \mathbf{0}, \mathbf{0}]^T$.

Figure 12 shows the state profiles with noise and the estimated state using Kalman filter. It is apparent that the temperature profile of wood chips are quite noisy in Figure 12 (a), while after applying the developed discrete-time Kalman filter, one can directly see that the noise has been filtered out, and the original state evolution is revealed as shown in Figure 12 (b). Although the temperature of wood chips and free liquor is coupled, in this case, the temperature of free liquor is relatively less affected by noise, therefore the profile of the estimated state for x_2 is not provided. By comparing the filtered state evolution with the original one (Figure 7), the effectiveness of the proposed discrete Kalman filter can be verified. From the comparison of outputs in Figure 13, one can noticed that the measured output profiles in the two figures are quite noisy, as shown in the black dashed lines, and the proposed Kalman filter can smooth out the noises in outputs and make the filtered output converge to real output profiles, as shown in green dashed lines and red solid lines, respectively.

To quantity the estimation performance of the proposed Kalman filter, the measurement error and the estimation error are calculated based on the actual outputs, as shown in Figure 14. The measurement error is defined as the difference between the measurement and the actual output, and the estimation error denotes the difference between the filtered output using Kalman filter and the actual output. The measurement error of both output are relatively random and large. After applying the Kalman filter, the estimated output 1 is close to the real output 1 as the estimation error is smooth and relatively small. Although the measurement error is largest when the time lag is around $100s$, the Kalman filter can also achieve relatively better estimation. As for output 2, the estimation performance is much better since the estimation error is converge to zero within $35s$ that might be caused by the spatially localized noise only appears in the temperature of wood chips or x_1.

4.2.2 Determination of Optimal sensor placement

We performed several simulation runs to evaluate the performance if the proposed method for computing optimal locations of measurement sensors. Each sensor have 6 possible locations distributed in the range $[0, 5]$ as shown in Table 2.

Based on the algorithm shown in Section 3, we compute the optimal sensor locations by minimizing the proposed cost function. By solving Equation (32), the optimal sensor locations can be determined. In this case, the optimal sensor locations were found at $\vartheta^* = [1, 3]$, where the minimum

cost was 181.5839. Figure 15 shows the distribution of the $\|P_{ss}\|_1$, and it can be seen that $\|P_{ss}\|_1$ is relatively large when the temperature sensor of free liquor is located close to the upper boundary (i.e., l_{m2} is small and close to 0). When the sensor is located far from the upper boundary, the value of trace becomes smaller and not much different from each other. The minimum value appears when the temperature sensor of free liquor is located at $3m$. The meaning behind this investigation is that it provides an efficient way and insightful guidance for practitioners when performing sensor location selection. However, when the feasible sensor location set has relatively large candidates, the computational cost will also increase by using the proposed method. The computation issue will be addressed in a future work.

5 CONCLUSION

In summary, the state estimation and sensor placement for the stochastic continuous pulp digester with measurement delay are investigated in this work from the monitoring point of view. The temperature system of a continuous pulp digester is modeled by two coupled hyperbolic partial differential equations and an ordinary differential equation, and there exists the measurement delay at the considered outputs. In order to realize discrete implementation, the Cayley-Tustin transform is utilized to map the continuous-time system to the discrete-time model representation without spatial discretization and model reduction which preserves the input-output stability of the plant. The discrete-time infinite-dimensional Kalman filter is applied to estimate the system states using the process measurements. The selection of sensor location is then addressed based on the estimator design and investigated by minimizing the variance of estimate error. The effectiveness and feasibility of the proposed Kalman filter are verified by a set of simulations, and the results of the determination of optimal sensor placement provided an efficient way and insightful guidance for practitioners when performing sensor location selection.

Literature Cited

1. M. Rahman, A. Avelin, and K. Kyprianidis, An approach for feedforward model predictive control of continuous pulp digesters, *Processes*, vol. 7, no. 9, p. 602, 2019.

2. ——, A review on the modeling, control and diagnostics of continuous pulp digesters, *Processes*, vol. 8, no. 10, p. 1231, 2020.

3. C. Smith, Studies of the mathematical modelling, simulation, and control of the operation of a kamyr continuous digester for the kraft process, *Purdue University: West Lafayette, Indiana, USA*, 1974.

4. R. R. Gustafson, C. A. Sleicher, W. T. McKean, and B. A. Finlayson, Theoretical model of the kraft pulping process, *Industrial & Engineering Chemistry Process Design and Development*, vol. 22, no. 1, pp. 87–96, 1983.

5. N. Andersson, Modelling of kraft cooking kinetics using near infrared spectroscopy, Ph.D. dissertation, Karlstad University Studies, 2003.

6. F. A. Michelsen and B. A. Foss, A comprehensive mechanistic model of a continuous kamyr digester, *Applied mathematical modelling*, vol. 20, no. 7, pp. 523–533, 1996.

7. P. A. Wisnewski, F. J. Doyle III, and F. Kayihan, Fundamental continuous-pulp-digester model for simulation and control, *AIChE journal*, vol. 43, no. 12, pp. 3175–3192, 1997.

8. S. Bhartiya, P. Dufour, and F. J. Doyle III, Fundamental thermal-hydraulic pulp digester model with grade transition, *AIChE journal*, vol. 49, no. 2, pp. 411–425, 2003.

9. J. Jung, H.-K. Choi, S. H. Son, J. S.-I. Kwon, and J. H. Lee, Multiscale modeling of fiber deformation: Application to a batch pulp digester for model predictive control of fiber strength, *Computers & Chemical Engineering*, vol. 158, p. 107640, 2022.

10. H.-K. Choi, S. H. Son, and J. Sang-Il Kwon, Inferential model predictive control of continuous pulping under grade transition, *Industrial & Engineering Chemistry Research*, vol. 60, no. 9, pp. 3699–3710, 2021.

11. J. H. Lee and A. Datta, Nonlinear inferential control of pulp digesters, *AIChE journal*, vol. 40, no. 1, pp. 50–64, 1994.

12. T. Clarke-Pringle and J. F. MacGregor, Reduced dimension control of dynamic systems, *Industrial & engineering chemistry research*, vol. 39, no. 8, pp. 2970–2980, 2000.

13. L. Ding, A. Johansson, and T. Gustafsson, Application of reduced models for robust control and state estimation of a distributed parameter system, *Journal of Process Control*, vol. 19, no. 3, pp. 539–549, 2009.

14. A. Alexandridis and H. Sarimveis, Nonlinear adaptive model predictive control based on self-correcting neural network models, *AIChE Journal*, vol. 51, no. 9, pp. 2495–2506, 2005.

15. F. J. Doyle III and F. Kayihan, Reaction profile control of the continuous pulp digester, *Chemical Engineering Science*, vol. 54, no. 13-14, pp. 2679–2688, 1999.

16. A. Alexandridis, H. Sarimveis, and G. Bafas, Modeling and control of continuous digesters using the pls methodology, *Chemical Engineering Communications*, vol. 191, no. 10, pp. 1271–1284, 2004.

17. N. Padhiyar, A. Gupta, A. Gautam, S. Bhartiya, F. J. Doyle III, S. Dash, and S. Gaikwad, Nonlinear inferential multi-rate control of kappa number at multiple locations in a continuous pulp digester, *Journal of Process Control*, vol. 16, no. 10, pp. 1037–1053, 2006.

18. T. J. Harris, J. Macgregor, and J. Wright, Optimal sensor location with an application to a packed bed tubular reactor, *AIChE Journal*, vol. 26, no. 6, pp. 910–916, 1980.

19. P. Müller and H. Weber, Analysis and optimization of certain qualities of controllability and observability for linear dynamical systems, *Automatica*, vol. 8, no. 3, pp. 237–246, 1972.

20. L. Meier, J. Peschon, and R. Dressler, Optimal control of measurement subsystems, *IEEE Transactions on Automatic Control*, vol. 12, no. 5, pp. 528–536, 1967.

21. H. Kushner, Introduction to stochastic control: Technical report, Brown University Providence, RI Division of Applied Mathematics, Tech. Rep., 1971.

22. M. Van De Wal and B. De Jager, A review of methods for input/output selection, *Automatica*, vol. 37, no. 4, pp. 487–510, 2001.

23. U. Vaidya, R. Rajaram, and S. Dasgupta, Actuator and sensor placement in linear advection pde, in *2011 50th IEEE Conference on Decision and Control and European Control Conference*. IEEE, 2011, pp. 5395–5400.

24. M. Zhang and K. Morris, Sensor choice for minimum error variance estimation, *IEEE Transactions on Automatic Control*, vol. 63, no. 2, pp. 315–330, 2017.

25. D. W. Veldman, R. H. Fey, H. J. Zwart, M. M. van de Wal, J. D. van den Boom, and H. Nijmeijer, Sensor and actuator placement for proportional feedback control in advection-diffusion equations, *IEEE Control Systems Letters*, vol. 4, no. 1, pp. 193–198, 2019.

26. R. F. Curtain and J. C. Oostveen, Bilinear transformations between discrete-and continuous-time infinite-dimensional linear systems, North Carolina State University. Center for Research in Scientific Computation, Tech. Rep., 1997.

27. A. K. Singh and J. Hahn, Sensor location for stable nonlinear dynamic systems: Multiple sensor case, *Industrial & engineering chemistry research*, vol. 45, no. 10, pp. 3615–3623, 2006.

28. S. Bhartiya, P. Dufour, and F. J. Doyle III, Fundamental thermal-hydraulic pulp digester model with grade transition, *AIChE journal*, vol. 49, no. 2, pp. 411–425, 2003.

29. L. Ding, T. Gustafsson, and A. Johansson, Model parameter estimation of simplified linear models for a continuous paper pulp digester, *Journal of Process Control*, vol. 17, no. 2, pp. 115–127, 2007.

30. K. Pougatch, M. Salcudean, and I. Gartshore, A numerical model of the reacting multiphase flow in a pulp digester, *Applied mathematical modelling*, vol. 30, no. 2, pp. 209–230, 2006.

31. M. Krstic and A. Smyshlyaev, Backstepping boundary control for first-order hyperbolic pdes and application to systems with actuator and sensor delays, *Systems & Control Letters*, vol. 57, no. 9, pp. 750–758, 2008.

32. H. Sano, Stability analysis of heat exchangers with delayed boundary feedback, *Automatica*, vol. 127, p. 109540, 2021.

33. V. Havu and J. Malinen, The cayley transform as a time discretization scheme, *Numerical Functional Analysis and Optimization*, vol. 28, no. 7-8, pp. 825–851, 2007.

34. G. F. Franklin, J. D. Powell, M. L. Workman *et al.*, *Digital control of dynamic systems*. Addison-wesley Menlo Park, CA, 1998, vol. 3.

35. J. Xie, Q. Xu, D. Ni, and S. Dubljevic, Observer and filter design for linear transport-reaction systems, *European Journal of Control*, vol. 49, pp. 26–43, 2019.

36. D. Simon, *Optimal state estimation: Kalman, H infinity, and nonlinear approaches.* John Wiley & Sons, 2006.

37. L. Zhang, J. Xie, and S. Dubljevic, Dynamic modeling and model predictive control of a continuous pulp digester, *AIChE Journal*, vol. 68, no. 3, p. e17534, 2022.

List of Figures

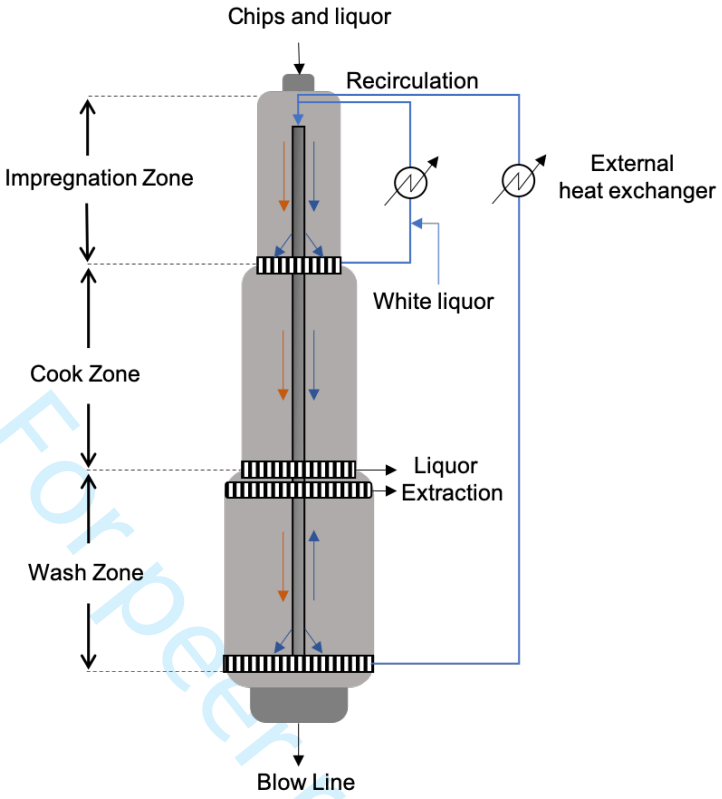

Figure 1: Simplified scheme of a continuous pulp digester[1]

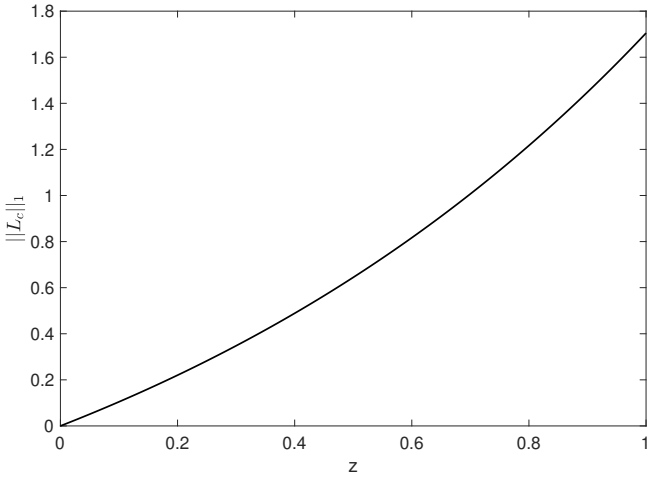

Figure 2: Trace norm of the observability gramian versus the single sensor location

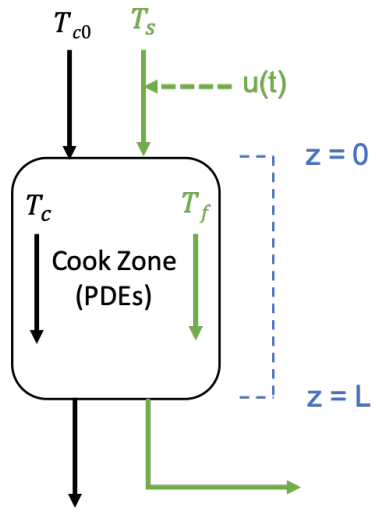

Figure 3: The scheme of cook zone in a pulp digester

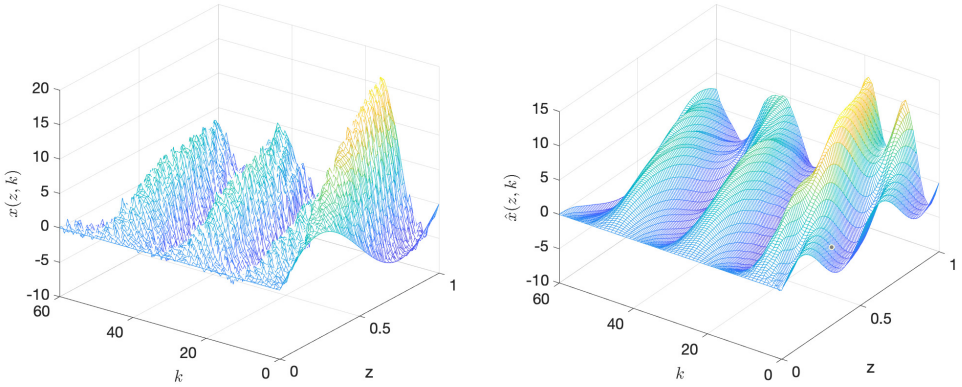

Figure 4: Profiles of the state with noise and the estimated state

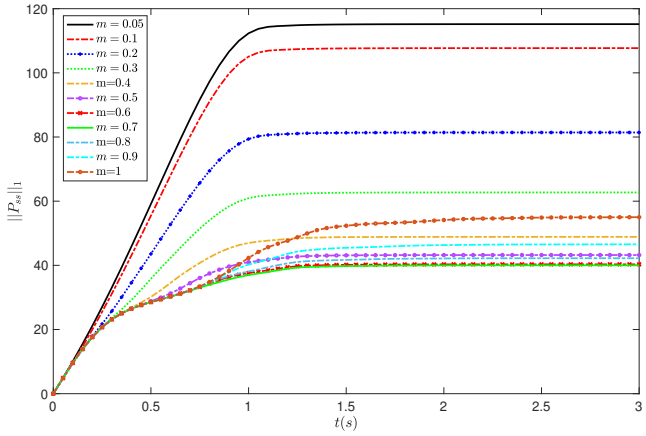

Figure 5: The convergency performance of the trace of the estimation error covariance

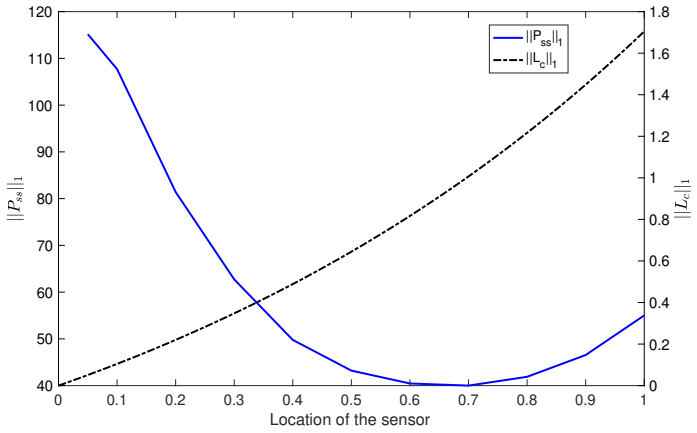

Figure 6: Comparison of the trace of steady-state estimation error covariance and trace of observability versus the spatial location of the sensor

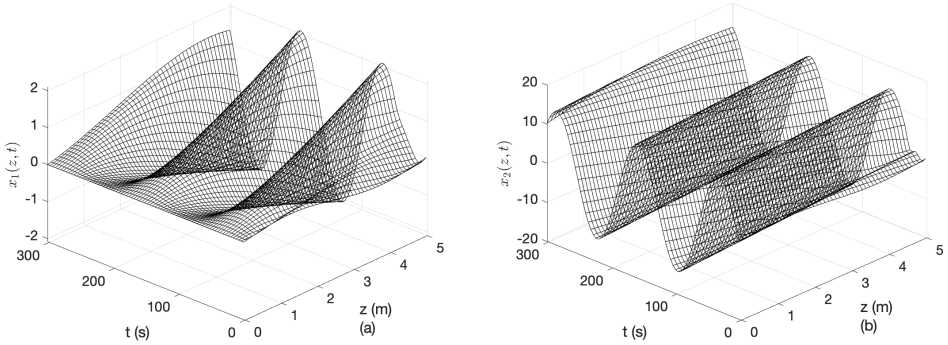

Figure 7: Perturbations of open-loop state profiles

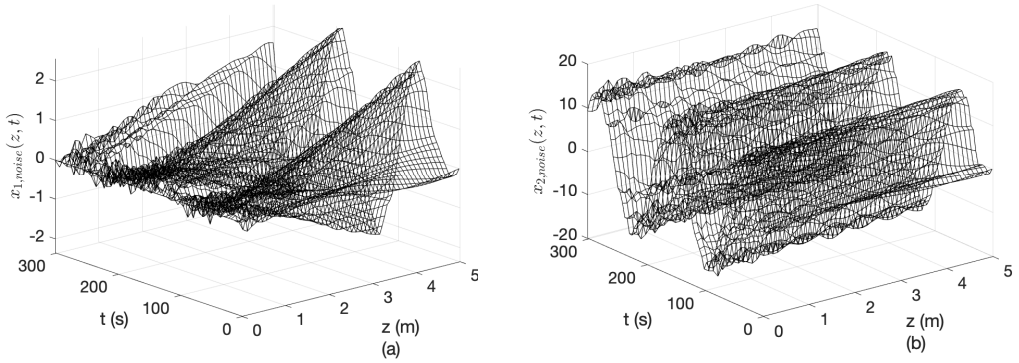

Figure 8: Profile of the states with noise

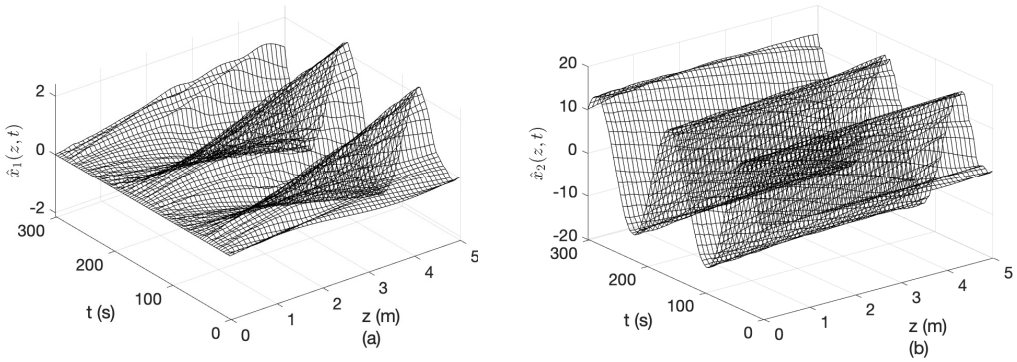

Figure 9: Profile of the estimated states

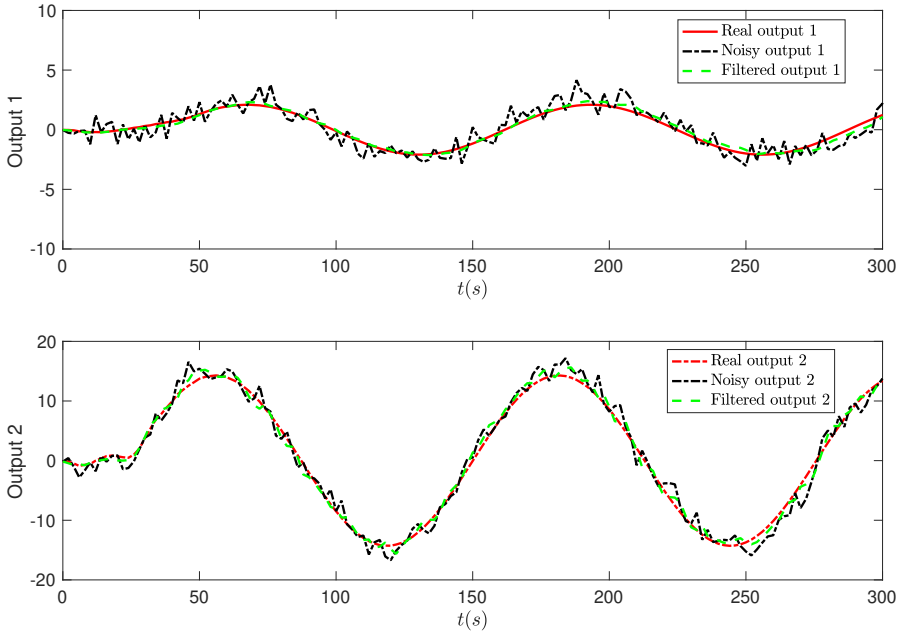

Figure 10: Filtering performance of outputs

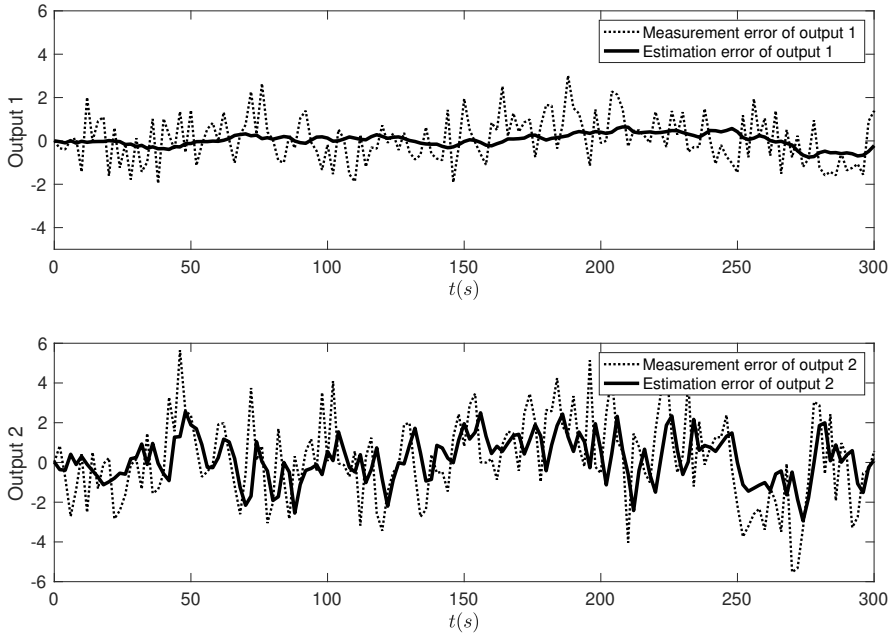

Figure 11: The measurement error and estimation error for case 1

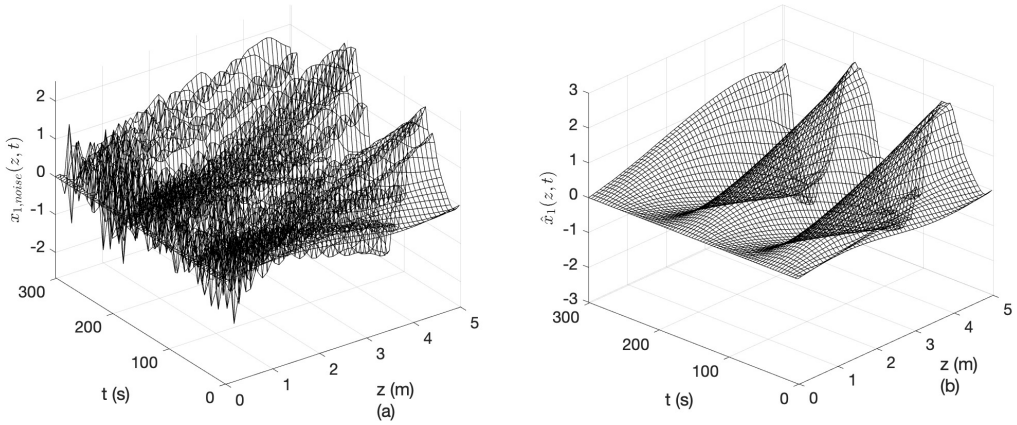

Figure 12: Profiles of the state with noise and the estimated states

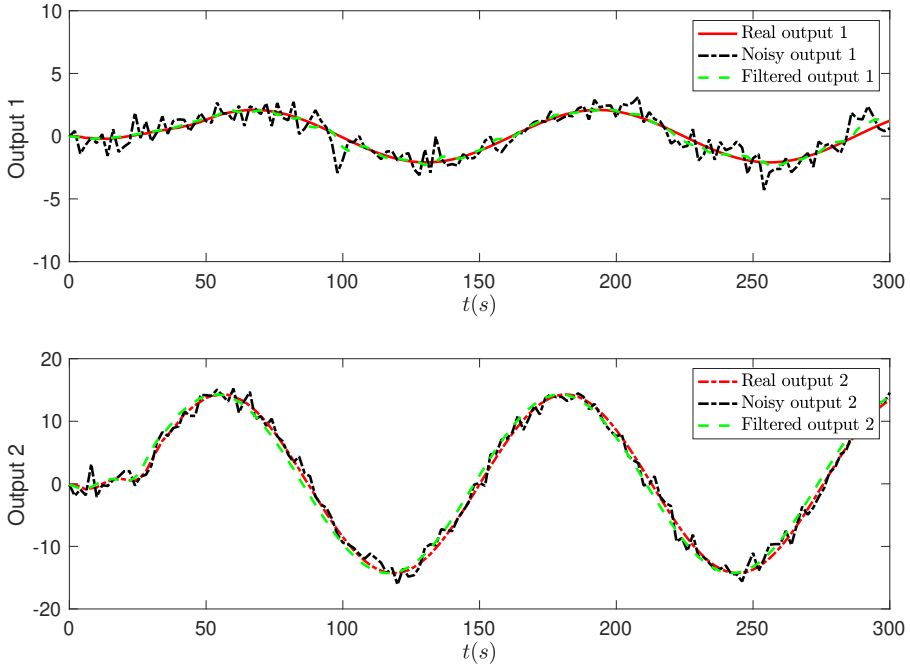

Figure 13: Filtering performance of output

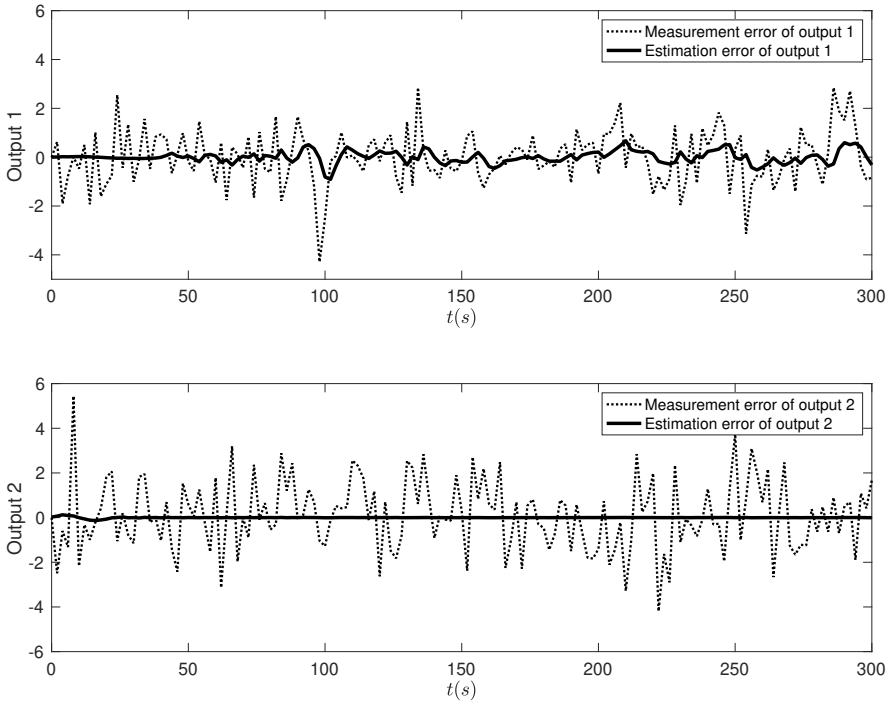

Figure 14: The measurement error and estimation error for case 2

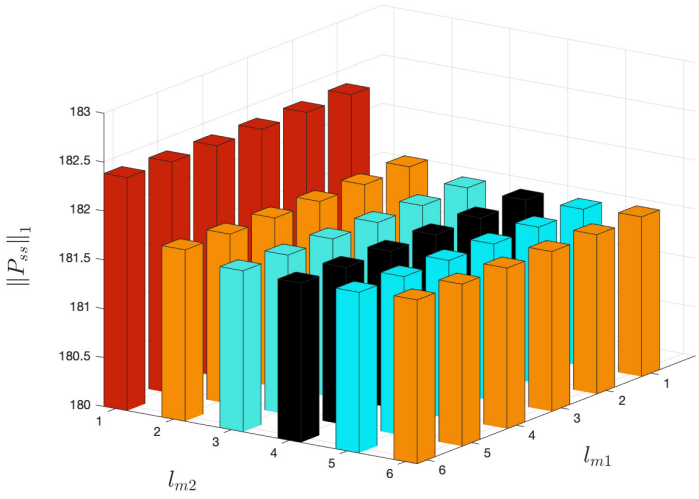

Figure 15: The trace norm values of different sensor locations under the consideration of given sensors location

List of Tables

Table 1: Notation and Values of Parameters[37]

Process parameters	Notations	Numerical Values
Volumetric flow rate of chip	V_c	0.0267 m^3/min
Volumetric flow rate of free liquor	V_f	0.09 m^3/min
Digester cross sectional area	A	21 m^2
Interphase heat-transfer coefficient	U	827 $kJ/min \cdot K \cdot m^3$
Heat capacities of the wood	C_{ps}	1.47 $kJ/kg \cdot K$
Heat capacities of the liquor	C_{pl}	4.19 $kJ/kg \cdot K$

Table 2: Locations considered for each sensor

Temperature locations of wood chips/l_{m1}	Temperature locations of free liquor/l_{m2}
0.2, 1, 2, 3, 4, 5	0.2, 1, 2, 3, 4, 5